Stapled Peptides Based on Human Angiotensin-Converting Enzyme 2 (ACE2) Potently Inhibit SARS-CoV-2 Infection *In Vitro*

Francesca Curreli,[a] Sofia M. B. Victor,[a] Shahad Ahmed,[a] Aleksandra Drelich,[b] Xiaohe Tong,[c] Chien-Te K. Tseng,[b,e] Christopher D. Hillyer,[d] Asim K. Debnath[a]

[a]Laboratory of Molecular Modeling & Drug Design, Lindsley F. Kimball Research Institute, New York Blood Center, New York, New York, USA
[b]Department of Microbiology and Immunology, The University of Texas Medical Branch, Galveston, Texas, USA
[c]CPS Scientific, Inc., San Jose, California, USA
[d]Lindsley F. Kimball Research Institute, New York Blood Center, New York, New York, USA
[e]Center of Biodefense and Emerging Disease, The University of Texas Medical Branch, Galveston, Texas, USA

ABSTRACT SARS-CoV-2 uses human angiotensin-converting enzyme 2 (ACE2) as the primary receptor to enter host cells and initiate the infection. The critical binding region of ACE2 is an ~30-amino-acid (aa)-long helix. Here, we report the design of four stapled peptides based on the ACE2 helix, which is expected to bind to SARS-CoV-2 and prevent the binding of the virus to the ACE2 receptor and disrupt the infection. All stapled peptides showed high helical contents (50 to 94% helicity). In contrast, the linear control peptide NYBSP-C showed no helicity (19%). We have evaluated the peptides in a pseudovirus-based single-cycle assay in HT1080/ACE2 cells and human lung cell line A549/ACE2, overexpressing ACE2. Three of the four stapled peptides showed potent antiviral activity in HT1080/ACE2 (50% inhibitory concentration [IC$_{50}$]: 1.9 to 4.1 μM) and A549/ACE2 (IC$_{50}$: 2.2 to 2.8 μM) cells. The linear peptide NYBSP-C and the double-stapled peptide StRIP16, used as controls, showed no antiviral activity. Most significantly, none of the stapled peptides show any cytotoxicity at the highest dose tested. We also evaluated the antiviral activity of the peptides by infecting Vero E6 cells with the replication-competent authentic SARS-CoV-2 (US_WA-1/2020). NYBSP-1 was the most efficient, preventing the complete formation of cytopathic effects (CPEs) at an IC$_{100}$ of 17.2 μM. NYBSP-2 and NYBSP-4 also prevented the formation of the virus-induced CPE with an IC$_{100}$ of about 33 μM. We determined the proteolytic stability of one of the most active stapled peptides, NYBSP-4, in human plasma, which showed a half-life ($T_{1/2}$) of >289 min.

IMPORTANCE SARS-CoV-2 is a novel virus with many unknowns. No vaccine or specific therapy is available yet to prevent and treat this deadly virus. Therefore, there is an urgent need to develop novel therapeutics. Structural studies revealed critical interactions between the binding site helix of the ACE2 receptor and SARS-CoV-2 receptor-binding domain (RBD). Therefore, targeting the entry pathway of SARS-CoV-2 is ideal for both prevention and treatment as it blocks the first step of the viral life cycle. We report the design of four double-stapled peptides, three of which showed potent antiviral activity in HT1080/ACE2 cells and human lung carcinoma cells, A549/ACE2. Most significantly, the active stapled peptides with antiviral activity against SARS-CoV-2 showed high α-helicity (60 to 94%). The most active stapled peptide, NYBSP-4, showed substantial resistance to degradation by proteolytic enzymes in human plasma. The lead stapled peptides are expected to pave the way for further optimization of a clinical candidate.

KEYWORDS angiotensin-converting enzyme 2 (ACE2), coronavirus disease 2019 (COVID-19), severe acute respiratory syndrome coronavirus 2 (SARS-CoV-2), hydrocarbon stapling, stapled peptides

A novel and highly pathogenic coronavirus named SARS-CoV-2 was first identified in Wuhan, China, in 2019. It causes coronavirus disease 2019 (COVID-19), and the resultant rapid global spread is a substantial threat to public health and the world economy. On 11 March 2020, the World Health Organization (WHO) declared the COVID-19 outbreak to be a global pandemic. As of 2 November 2020, 216 countries were affected by this disease (https://www.worldometers.info/coronavirus/countries -where-coronavirus-has-spread/), with more than 47 million positive cases, including more than 1.2 million deaths. In the United States, there are more than 9.2 million confirmed cases with more than 231,000 deaths (https://coronavirus.jhu.edu/data). At present, no vaccines or therapeutics are available to prevent or treat COVID-19. However, remdesivir and some corticosteroids, such as dexamethasone, are providing some benefit to COVID-19 patients. Several vaccines and other repurposed therapeutics are also in clinical trials. SARS-CoV-2, like its predecessor SARS-CoV, uses its receptor-binding domain (RBD) in the S1 spike protein to initiate entry by binding to human host receptor angiotensin-converting enzyme 2 (ACE2). Recently, soluble human ACE2 (hACE2) has been proposed as a competitive interceptor of SARS-CoV (1), and a recombinant hACE2 (rhACE2) is now undergoing a clinical trial (2). However, a recent report indicated that in both humans and mice, rACE2 had a high clearance rate, and the half-life was only hours in pharmacokinetic studies (3, 4). Recently, it was shown that when ACE2 was fused with an Fc fragment, ACE2-Ig, it showed high-affinity binding to the RBD of both SARS-CoV and SARS-CoV-2. ACE2-Ig also exhibited potent neutralization of SARS-CoV-2 with improved pharmacological properties in mice (5). Despite the potential of recombinant ACE2, in a dire global pandemic situation, protein-based therapy may not be suitable for use, especially in more-developing nations, primarily due to the high cost and instability of protein-based therapy. Therefore, we sought to design therapeutics that are more stable and less expensive to make for wider distribution. Recently, Zhang et al. (6) reported a 23-mer peptide (SBP1) from the ACE2 α1 helix sequence, which showed a potent binding affinity (K_D [equilibrium dissociation constant] = 47 nM) to the SARS-CoV-2 RBD. However, there was no antiviral activity data reported (6). We envision that this type of short linear peptide will not be stable against proteolysis and, most significantly, may not have the right secondary structure required for efficient binding with the SARS-CoV-2 RBD.

Recent cryo-electron microscopy (cryo-EM) and X-ray structures of the SARS-CoV-2 RBD with full-length ACE2 revealed structural details of the binding interactions of these two proteins (7–10). A close inspection revealed that the interaction surface is long and flat, which may not be conducive to design small-molecule drugs to prevent protein-protein interactions. Interestingly, however, the structure also revealed that one of the long α-helices (here termed Helix-1) interacts with the RBD consisting of multiple binding "hot spots." Based on this structural insight, we designed stapled peptides based on the binding site of SARS-CoV-2 RBD on the ACE2 receptor (Helix-1), which are expected to act as a decoy receptor preventing the binding of SARS-CoV-2 to the host receptor ACE2 (Fig. 1) and hence virus entry to host cells. Targeting the entry pathway of SARS-CoV-2 is ideal for both prevention and treatment as it blocks the first step of the viral life cycle.

Protein-protein interactions (PPI) between host and virus are valuable targets to inhibit viral replication. However, the large and flat interacting surfaces of PPI often preclude the use of small molecules as drugs to disrupt these PPI. Larger biologics, such as peptidomimetics (e.g., hydrocarbon-stapled-peptide mimetics), are, on the other hand, promising inhibitors of PPI that were previously intractable (11–14). Stapled peptides are typically derived from the α-helix from the binding interface, and they are locked into bioactive conformations through the use of chemical linkers. Stapling enhances α-helicity of unstructured short peptides in solution, improves resistance against proteolytic digestion, as well as potency, and often improves cell penetration (15–21). One of these stapled peptides, ALRN-6924, is in various clinical trials for the treatment of lymphomas (phase 1b/2), peripheral T-cell lymphoma (phase 2a), acute
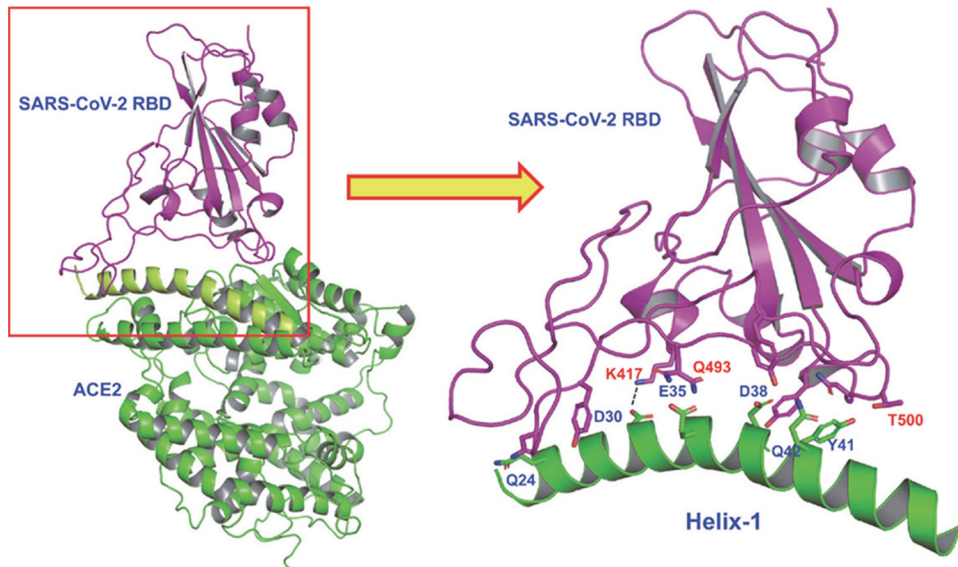
FIG 1 X-ray structure showing binding of SARS-CoV-2 RBD (violet) with ACE2 receptor (green). The detailed interactions of Helix-1 of ACE2 with SARS-CoV-2 RBD are indicated in the illustration on the right.

myeloid lymphoma (AML, phase 1), and advanced myelodysplastic syndrome (MDS, phase 1) (22).

Here, we took advantage of Helix-1 of ACE2 to design peptide-based therapeutics for COVID-19. However, Helix-1 is expected to lose its helical conformation in solution; therefore, it will also lose the orientation of most, if not all, of the binding site residues to make any proper interaction. To counter this, we adopted the very-well-studied concept of hydrocarbon stapling techniques mentioned above to reinforce the bioactive helical conformation of Helix-1 (Fig. 2). We hypothesize that stapled peptides will be α-helical and will be proteolytically stable. They are expected to bind to the SARS-CoV-2 RBD and inhibit virus entry to cells.

In this report, we present the design of four such stapled peptides based on Helix-1 of ACE2. Three of these peptides showed potent SARS-CoV-2-inhibitory activity in an *in vitro* pseudovirus and in an authentic virus infectivity assay. These stapled peptides have potential as a therapeutic for COVID-19 by functioning as a decoy of the ACE2 binding site for SARS-CoV-2 and preventing the virus from binding to the ACE2 receptor, thereby preventing virus entry and infection.

RESULTS AND DISCUSSION

Design of double-stapled peptides. Structures recently solved by cryo-EM and X-rays provided intricate details on how SARS-CoV-2 RBD binds to the host receptor ACE2. The major binding sites are located on Helix-1 of ACE2 (Fig. 1). A recent report indicated that a computationally designed short peptide from Helix-1 of ACE2 showed a nanomolar binding affinity to SARS-CoV-2 RBD (6). However, the usefulness of such a linear peptide in isolation as a drug is yet to be proven. In general, when a helix is taken out as a peptide from a protein, it loses its secondary structure. These peptides are also prone to proteolytic degradation. In contrast, if such small peptides are constrained by hydrocarbon stapling, an enhancement of helical content can be achieved together with resistance to proteolysis and improved binding affinity and biological activity (11–21, 23, 24). Therefore, we envisioned that the stapling of Helix-1 would render it α-helical, resistant to proteolysis, and, therefore, a highly potent inhibitor of SARS-CoV-2.

***i/i+4* and *i/i+7* hydrocarbon stapling.** We used the well-established stapling techniques to synthesize hydrocarbon-stapled peptides (25–27) from Helix-1 of ACE2, which are expected to maintain high α-helicity, have high binding affinity to SARS-
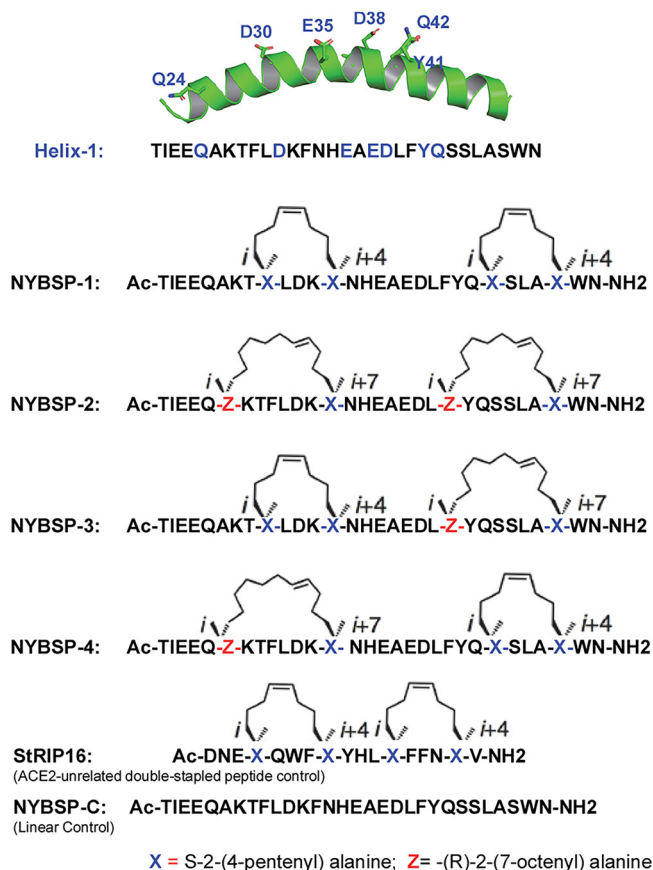
FIG 2 Design of double-stapled peptides as anti-SARS-CoV-2 inhibitors. The linear peptide, NYBSP-C, and an ACE2-unrelated double-stapled peptide, StRIP16 (29), were used as controls.

CoV-2 RBD, and have improved antiviral activity and stability from proteolysis. We decided to use double stapling because of the relatively longer helical region that binds to the SARS-CoV-2 RBD. Double stapling has been reported to confer striking protease resistance (20, 28, 29). Furthermore, Mourtada et al. recently reported 2- to 4-fold enhancement of antimicrobial potency by double-stapled peptides over single stapling (23). Double stapling was also reported to achieve improved pharmacokinetic profiles, including oral absorption of peptide-based HIV-1 fusion inhibitors (28). For the *i,i+4* and *i,i+7* stapling, we used nonnatural amino acids as illustrated in Fig. 2 to introduce the hydrocarbon staples to Helix-1. The stapling sites were selected based on the binding site information of SARS-CoV-2 RBD with ACE2 (Helix-1) from the cryo-EM and X-ray structure mentioned above so that they do not interfere with the critical binding site residues. We have synthesized (CPC Scientific, Inc.) four stapled peptides, as depicted in Fig. 2. We also synthesized the linear peptide NYBSP-C as a control. Besides, we purchased StRIP16 (29), which is a Rab8a GTPase-binding double-stapled peptide and unrelated to ACE2, to use as a control.

Effect of double stapling on the helical propensity. Due to the extended size of Helix-1, we decided to double staple Helix-1 of ACE2 to preserve the α-helical content of the peptides. To determine the helical propensity of these peptides, we resorted to circular dichroism (CD) spectroscopy for analyzing secondary structures. The data in Fig. 3A indicate that all the stapled peptides had the maxima at 190 nm and two minima at 208 and 222 nm, confirming that all these stapled peptides had α-helical structure. The percent helicity calculation shows remarkable improvement over the linear peptide. The data in Fig. 3B indicate that NYBSP-1 had the highest helical propensity of
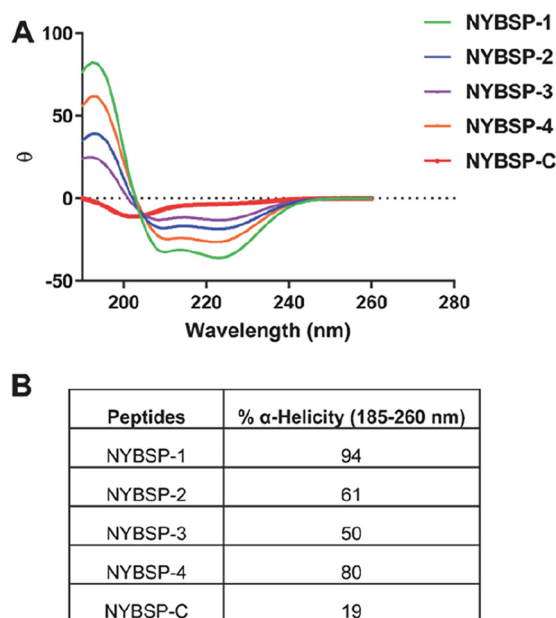
FIG 3 α-Helical propensity measured by CD spectroscopy. (A) CD spectra. (B) Percent helicity of the double-stapled peptides and the linear control peptide.

94%. Stapled peptides NYBSP-2 and NYBSP-4 had percent helicities of 61 and 80, respectively. NYBSP-3 showed the lowest percent helicity (50%) among the four stapled peptides. The control peptide, NYBSP-C, as expected, showed no indication of α-helical propensity, with only 19% helicity. The control stapled peptide, StRIP16, was reported to have 38% helicity (29).

Binding affinity of a double-stapled peptide by SPR analysis. We used surface plasmon resonance (SPR) to determine the binding affinity of one double-stapled peptide, NYBSP-4, with SARS-CoV-2 RBD. This method is useful in measuring the binding constant (K_D) as well as k_{on} (also known as association constant, k_a) and k_{off} (also known as dissociation constant, k_d). We also used the linear peptide NYBSP-C as a control. Various concentrations of biotinylated SARS-CoV-2 RBD were manually printed onto the chip (immobilization) via biotin-avidin conjugation. Peptides were passed through the chip surface, and the signal changes (in arbitrary units [AU]) of each peptide at varied concentrations were recorded (Fig. 4A and B). The resulting data were fit to a 1:1 binding model, and the binding affinity K_D and kinetic parameters k_{on} and k_{off} of the interaction of SARS-CoV-2 RBD with NYBSP-C and NYBSP-4 were determined (Fig. 4C). The K_D value of NYBSP-4 was 2.2 μM, which was very much in line with the antiviral activity we observed against SARS-CoV-2 pseudovirus (Table 1). As expected, the linear peptide NYBSP-C, used as a control, showed poor binding (73.7 μM), which was about 33.5-fold lower than NYBSP-4. The SPR analysis also confirmed that the double-stapled peptides bind directly to the SARS-CoV-2 RBD.

Proteolytic stability of stapled peptides in human plasma. Proteolytic stability remains a potential concern in developing peptide-based therapy. We wanted to address this problem by introducing double stapling in Helix-1 of the ACE2 receptor. Double stapling is known to enhance protection from proteolysis. However, it was prudent for us to test how the stapled peptides that we designed withstand proteolysis in human plasma. The peptides were incubated with human plasma at 37°C, and the fragments formed from proteolysis were measured by liquid chromatography-tandem mass spectrometry (LC-MS/MS) at different time points (0, 10, 30, 60, and 120 min). We used a small-molecule drug, propantheline bromide, as an assay control. The data in Fig. 5 show that stapled peptide NYBSP-4 is highly stable during the time used for the assay. The calculated half-life ($T_{1/2}$) of NYBSP-4 was >289 min, but surprisingly, the
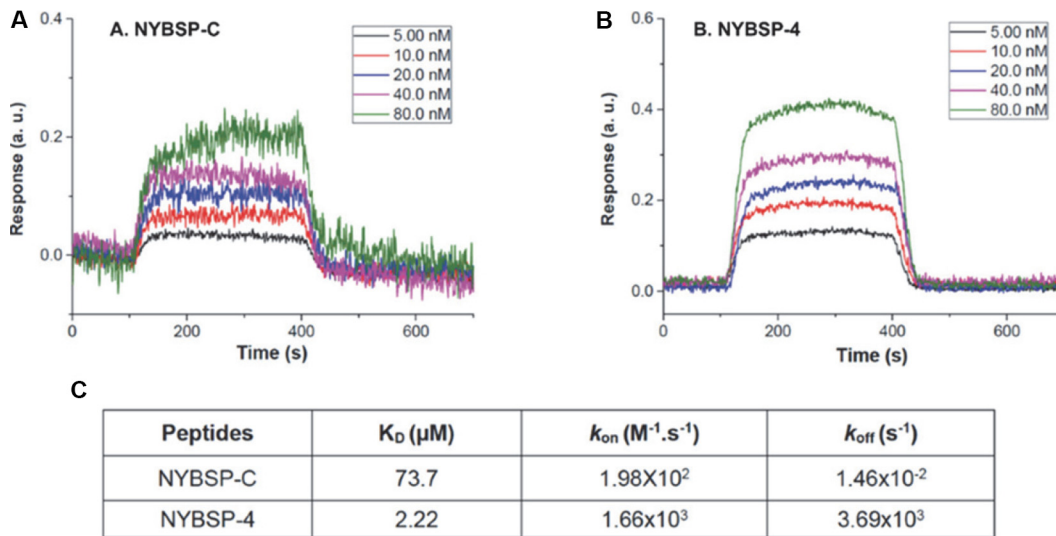
FIG 4 Evaluation of binding affinity of peptides to SARS-CoV-2 RBD by SPR. Kinetics fitting curve (sensogram) of SARS-CoV-2 RBD to NYBSP-C, a linear control peptide (A); NYBSP-4, a double-stapled peptide (B); and the binding affinity K_D and kinetic parameters k_{on} and k_{off} of NYBSP-C and NYBSP-4 (C).

linear control peptide NYBSP-C also showed similar stability ($T_{1/2} >$289 min). Usually, small peptides are known to get proteolytically cleaved quickly. The unusual stability of the linear peptide in human plasma in our test is yet to be understood.

Validation of the SARS-CoV-2 pseudovirus. We prepared SARS-CoV-2 pseudovirus capable of single-cycle infection by transfecting HEK293T/17 cells with an HIV-1 Env-deleted proviral backbone plasmid, pNL4-3ΔEnv-NanoLuc, and pSARS-CoV-2-S$_{\Delta 19}$ plasmid (30). The incorporation of the spike protein in the pseudovirus was validated by Western blot analysis using the SARS spike protein antibody (Novus Biologicals) (Fig. 6A). This antibody targets explicitly amino acids 1124 to 1140 of the spike protein S2. We found a specific band at 80 kDa, which identifies the subunit S2, and a second band at about 190 kDa, which corresponds to the full-length S protein (S1 + S2), as previously reported (31, 32), confirming the incorporation of the SARS-CoV-2 S protein in the pseudovirus. Moreover, the correlation of SARS-CoV-2 pseudovirus with the expression of the ACE2 receptor was analyzed by infecting five different cell types including human fibrosarcoma HT1080 cells overexpressing ACE2 (HT1080/ACE2) and the parental HT1080 cell type, human lung carcinoma A549 cells overexpressing ACE2 (A549/

TABLE 1 Antiviral activity (IC$_{50}$) of peptides in single-cycle assay in HT1080/ACE2 and A549/ACE2 cells infected with pseudoviruses (NL4-3ΔEnv-NanoLuc/SARS-CoV-2 and NL4-3.Luc.R-E-/VSV-G) and cytotoxicity (CC$_{50}$)

Peptide	HT1080/ACE2 cells			A549/ACE2 cells		
	IC$_{50}$ (μM)[a]			IC$_{50}$ (μM)[a]		
	SARS-CoV-2	VSV-G	CC$_{50}$ (μM)[a]	SARS-CoV-2	VSV-G	CC$_{50}$ (μM)[a]
NYBSP-1	4.1 ± 0.26	>27.5	>27.5[b]	2.2 ± 0.14	>27.5	>27.5[b]
NYBSP-2	2.9 ± 0.27	>26.8	>26.8[b]	2.68 ± 0.14	>26.8	>26.8[b]
NYBSP-3	12.9 ± 0.35	>27.6	>27.6[b]	~25	>27.6	>27.6[b]
NYBSP-4	1.97 ± 0.14	>26.6	>26.6[b]	2.8 ± 0.08	>26.6	>26.6[b]
NYBSP-C[c]	>27.7	>27.7	>27.7[b]	>27.7	>27.7	>27.7[b]
StRIP16[d]	>43.5	>43.5	>43.5[b]	>43.5	>43.5	>43.5[b]
Anti-ACE2	<70 ng/ml	>5 μg/ml	>5 μg/ml[b]	<70 ng/ml	>5 μg/ml	>5 μg/ml[b]

[a]The reported IC$_{50}$ and CC$_{50}$ values represent the means ± standard deviations ($n = 3$).
[b]Less than 10% toxicity at this dose.
[c]NYBSP-C, a linear peptide from Helix-1, was used as a control.
[d]StRIP16, an ACE2-unrelated Rab8a GTPase-binding double-stapled peptide reported earlier (29), was used as a control.
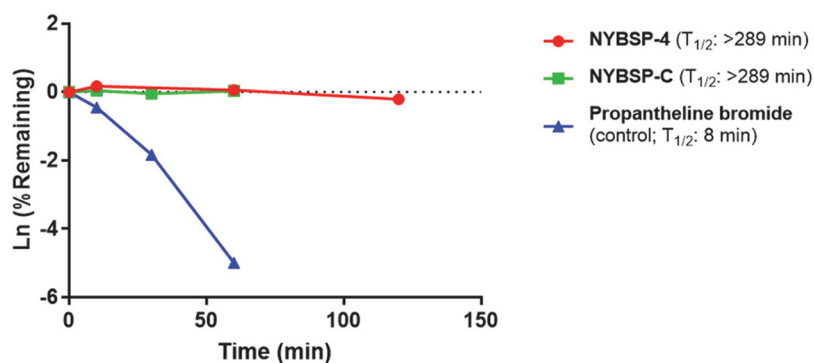
FIG 5 The plasma stability of double-stapled peptide NYBSP-4 (red) and control linear peptide NYBSP-C (green). Propantheline bromide (a small-molecule antimuscarinic agent) was used as an assay control.

ACE2) and the parental A549 cell type, and HeLa cells which do not express hACE2. The cells were infected with the same volumes of the supernatant-containing pseudovirus SARS-CoV-2. As expected, we found no infection of the HeLa cells (Fig. 6B), while we detected a low level of infection of the HT1080 and A549 cells (1.5×10^5 and 9.2×10^4 relative luminescence units [RLU], respectively). The HT1080/ACE2 supported high levels of SARS-CoV-2 infection. In fact, we detected about 10^8 RLU, which corresponds to a 665-fold-higher infection than what we detected for the parental cell type HT1080. The infection detected for the A549/ACE2 cells was moderate (about 8×10^5 RLU) compared to that for HT1080/ACE2 but about 9-fold higher than what we detected for the parental cell type A549. These results were confirmed by analyzing the expression levels of the ACE2 receptor in the different cell lines by Western blotting (Fig. 6C). As shown in Blot-1, we found that ACE2 expression was undetectable in the parental cell line HT1080, while it was overexpressed in HT1080/ACE2 cells. The lower infection detected in A549/ACE2 cells suggested a lower ACE2 expression in these cells. For this reason, in Blot-2, we loaded a larger amount of proteins (75 μg). As expected, the expression levels of ACE2 were undetectable in the parental cell line A549 and the HeLa cells. The expression was moderate in the A549/ACE2 cells compared to HT1080/ACE2. These data confirmed that SARS-CoV-2 pseudovirus infects the cells through its interaction with the ACE2 receptor.

Anti-SARS-CoV-2 activity and cytotoxicity of double-stapled peptides in cell-based assays. We evaluated the anti-SARS-CoV-2 activity of the double-stapled peptides by infecting the two cell types overexpressing hACE2, the human fibrosarcoma HT1080/ACE2 cells and the human lung carcinoma A549/ACE2 cells, with a SARS-CoV-2 pseudovirus that was pretreated with escalating concentrations of the peptides for 30 min. The linear peptide NYBSP-C, an unrelated double-stapled peptide (StRIP16) (29), and an anti-ACE2 monoclonal antibody (Mab) (AC384 from AdipoGen Life Sciences) were used as controls. The concentration required to inhibit 50% (IC_{50}) of SARS-CoV-2 pseudovirus infection was calculated. The results are shown in Table 1. The dose-response plots (Fig. 7) indicate that all the double-stapled peptides efficiently inhibited the infection of HT1080/ACE2 cells and A549/ACE2 cells by the SARS-CoV-2 pseudovirus with low-micromolar potency. Three of the four stapled peptides displayed potent antiviral activity in both cell lines. The IC_{50}s in HT1080/ACE2 and A549/ACE2 cells for NYBSP-1 were 4.1 ± 0.26 and 2.2 ± 0.14, for NYBSP-2 were 2.9 ± 0.27 and 2.68 ± 0.14, and for NYBSP-4 were 1.97 ± 0.14 and 2.8 ± 0.08 μM, respectively. NYBSP-3 was the least active peptide with an IC_{50} of 12.9 ± 0.35 μM in HT1080/ACE cells and $\sim$25 μM in A549/ACE2 cells. Most significantly, as expected, neither of the two controls, the linear peptide NYBSP-C and the double-stapled peptide StRIP16, showed any antiviral activity while the IC_{50} detected for the anti-ACE2 MAb was <70 ng/ml (at this concentration, we detected about 65 to 80% viral inhibition). It is interesting that NYBSP-3 had the lowest percent α-helicity among all the stapled peptides designed, and it also showed

A.

B.

C.

Blot-1

Blot-2
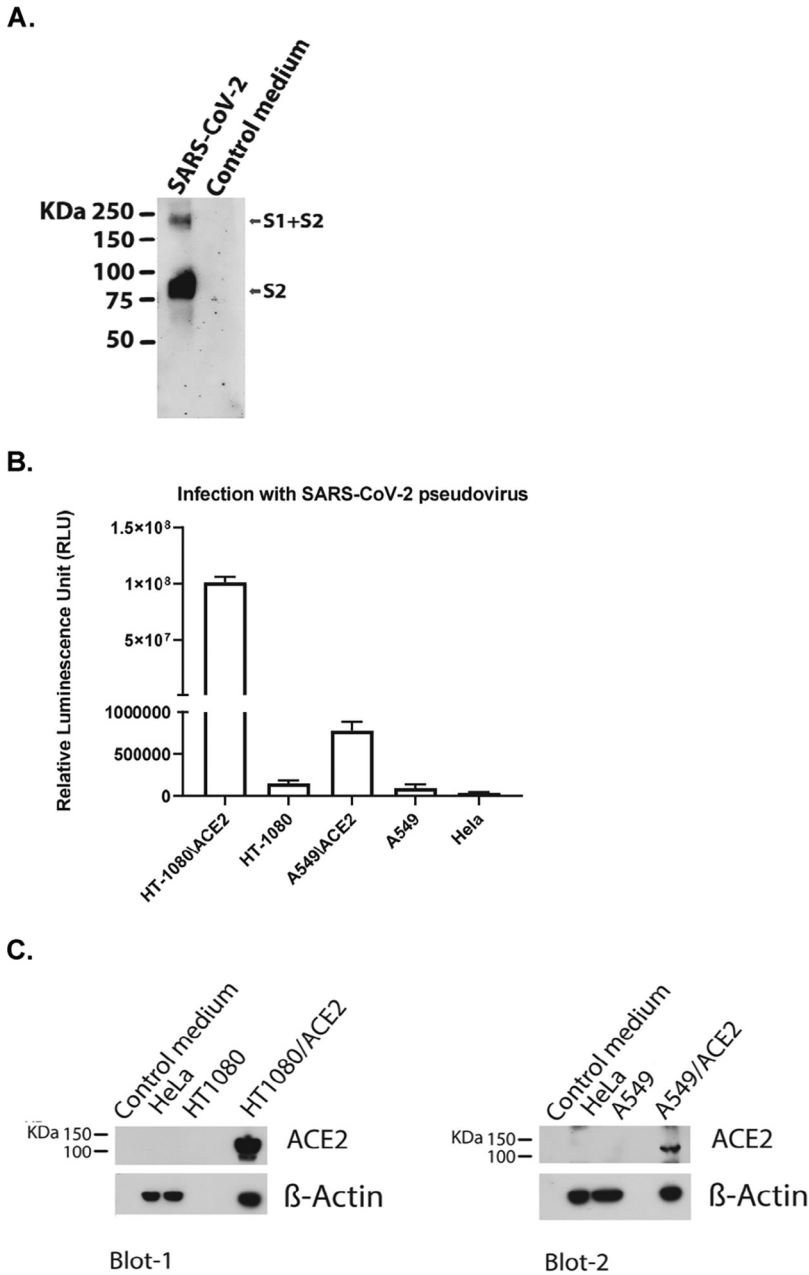
FIG 6 Validation of SARS-CoV-2 pseudovirus and ACE2 expression in different cells. (A) Western blot analysis to validate the incorporation of the S spike protein in the SARS-CoV-2 pseudovirus using the SARS spike protein antibody (Novus Biologicals), which targets the spike protein S2. (B) Infection of cells expressing different levels of ACE2, with the same amounts of SARS-CoV-2 pseudovirus. Columns represent the means ± standard deviations ($n = 3$). (C) Immunoblot analysis of cell lysates to evaluate ACE2 expression. β-Actin was used as a loading control.

the least antiviral activity. Moreover, none of the peptides showed activity against the control pseudovirus vesicular stomatitis virus glycoprotein (VSV-G) (Table 1), suggesting that their inhibitory activity is specific to SARS-CoV-2.

The 50% cytotoxicity (CC_{50}) of the peptides was assessed in parallel with the inhibition assays. We found that the peptides did not induce any apparent cell toxicity at the highest dose tested. More specifically, <10% toxicity was detected at the higher dose used in this assay (Table 1).

Additionally, the antiviral activity of the peptides was evaluated by infecting Vero

A. % Inhibition in HT1080/ACE2 Cells

B. % Inhibition in A549/ACE2 Cells
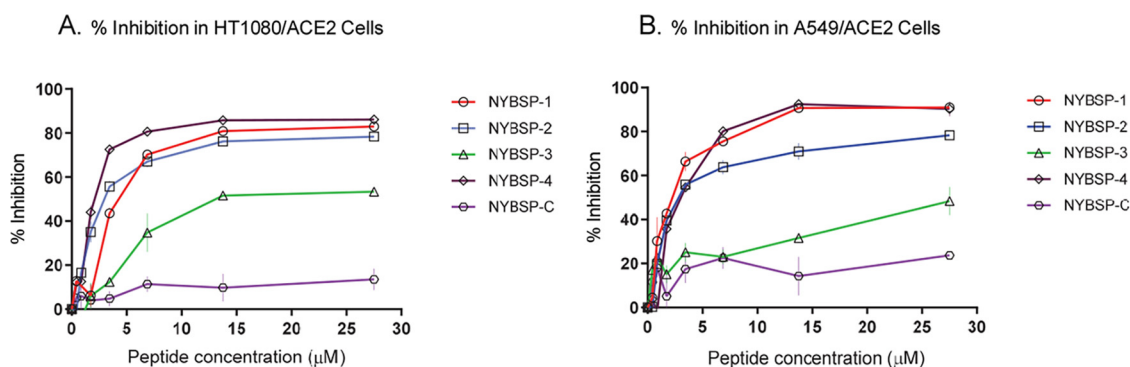
FIG 7 Dose-response plots of the antiviral activity of peptides in a single-cycle assay performed in HT1080/ACE2 and A549/ACE2 cells infected with pseudovirus NL4-3ΔEnv-NanoLuc/SARS-CoV-2. Antiviral activity in HT1080/ACE2 cells (A) and A549/ACE2 cells (B). Data on stapled peptides NYBSP-1, NYBSP-2, NYBSP-3, and NYBSP-4 and control linear peptide NYBSP-C are shown as mean ± SD from three independent experiments.

E6 cells with the replication-competent virus SARS-CoV-2 (US_WA-1/2020). The cells were observed under the microscope after 4 days of incubation to evaluate the formation of virus-induced cytopathic effect (CPE), and the efficacy of the peptides was expressed as the lowest concentration capable of completely preventing virus-induced CPE (IC_{100}). We found that the linear peptide NYSBP-C and the double-stapled NYBSP-3 did not completely prevent the formation of the virus-induced CPE at the highest dose used in this assay (Table 2), while NYBSP-1 was the most efficient in preventing the complete formation of CPEs at an IC_{100} of 17.2 μM. NYBSP-2 and NYBSP-4 also prevented the formation of the virus-induced CPE with an IC_{100} of about 33 μM.

MATERIALS AND METHODS

Peptide synthesis: general procedure of coupling. Fmoc (9-fluorenylmethoxy carbonyl) Rink amide MBHA resin (0.1 mmol) was swelled in dimethylformamide (DMF) (20 ml) for 1 h. The suspension was filtered. Twenty percent piperidine in DMF (20 ml) was added to the resin to remove Fmoc. The suspension was kept at room temperature for 0.5 h, while a stream of nitrogen was bubbled through it. The mixture was filtered, and the resin was washed with DMF (6 × 20 ml). Fmoc-Asn(Trt)-OH (0.3 mmol) was preactivated with N,N'-diisopropylcarbodiimide (DIC) (0.3 mmol) and hydroxybenzotriazole (HOBt) (0.3 mmol) in 10 ml DMF, and then the mixture was added into the resin. The reaction was carried out in a nitrogen atmosphere. The Kaiser ninhydrin test was used to indicate reaction completion. After the reaction was completed, the suspension was filtered, and the resin was washed with DMF (3 × 20 ml). After that, all sequences of amino acids were coupled and completed to give the peptidyl resin full protection, which was used to do the cyclization with Grubbs first catalyst.

The peptidyl resin was washed with DCM (3 × 20 ml). Then, 10 ml 1,2-dichloroethane was added in the reaction vessel, and the solution was bubbled by N_2. Fifteen minutes later, 30 mg of Grubbs first catalyst was added to the reaction vessel and bubbled by N_2 for 4 h and filtered, and the resin was washed with methanol (MeOH) (2 × 150 ml), DCM (2 × 150 ml), and MeOH (2 × 150 ml). The resin was dried under vacuum overnight to give cyclized peptidyl resin.

E solution (trifluoroacetic acid [TFA]-thioanisole-phenol-ethanedithiol [EDT]-H_2O = 87.5:5:2.5:2.5:2.5, 350 ml) was added into the peptidyl resin, and the suspension was shaken for 3.5 h followed by filtration. Ether (2,000 ml) was added into the filtrate, and peptide was precipitated. The mixture was centrifuged, and the ether layer was decanted. The peptide was washed three times with ether and dried under vacuum overnight to give the crude peptide.

TABLE 2 Antiviral activity (IC_{100}) of peptides in Vero E6 cells infected with SARS-CoV-2 (US_WA-1/2020)

Peptide	IC_{100} (μM)[a]
NYBSP-1	17.2
NYBSP-2	33.5
NYBSP-3	NA[b]
NYBSP-4	33
NYBSP-C	NA[b]

[a]Values indicate the lowest concentration capable of completely preventing virus-induced CPE in 100% of the wells.
[b]NA means the presence of CPE at the highest concentration.

All crude peptides were purified by pre-high-performance liquid chromatography (pre-HPLC) to >90% purity. They were acetylated at the C terminus and amidated at the N terminus. The molecular weight of all peptides was confirmed by electrospray mass spectrometry.

Circular dichroism spectroscopy. The secondary structure analysis to calculate percent α-helicity was performed by Creative Biolabs (New York, NY, USA). In brief, peptides were dissolved in 10 mM phosphate-buffered saline (PBS) to make a final concentration of 0.125 mg/ml in PBS. The CD spectra were obtained on a Chirascan spectropolarimeter (Applied Photophysics, Leatherhead, United Kingdom). The measurement parameters were set up as follows: wavelength, 185 to 260 nm; step size, 0.5 nm; temperature, 25°C. The percent helicity was calculated using the software CDNN (Circular Dichroism analysis using Neural Networks) (http://gerald-boehm.de/download/cdnn) (33).

SPR analysis. The binding study of one double-stapled peptide, NYBSP-4, and the linear control peptide, NYBSP-C, was performed by Profacgen, New York, NY. The bare gold-coated (thickness, 47 nm) PlexArray Nanocapture sensor chip (Plexera Bioscience, Seattle, WA, USA) was prewashed with 10× PBS-Tween (PBST) for 10 min, 1× PBST for 10 min, and deionized water twice for 10 min before being dried under a stream of nitrogen prior to use. Various concentrations of biotinylated recombinant SARS-CoV-2 spike RBD protein (Bioss Antibodies, Woburn, MA) dissolved in water were manually printed onto the chip with Biodo bioprinting at 40% humidity via biotin-avidin conjugation. Each concentration was printed in replicate, and each spot contained 0.2 μl of the sample solution. The chip was incubated in 80% humidity at 4°C overnight and rinsed with 10× PBST for 10 min, 1× PBST for 10 min, and deionized water twice for 10 min. The chip was then blocked with 5% (wt/vol) nonfat milk in water overnight and washed with 10× PBST for 10 min, 1× PBST for 10 min, and deionized water twice for 10 min before being dried under a stream of nitrogen prior to use. SPR imaging (SPRi) measurements were performed with PlexArray HT (Plexera Bioscience, Seattle, WA, USA). Collimated light (660 nm) passes through the coupling prism, reflects off the SPR-active gold surface, and is received by the charge-coupled device (CCD) camera. Buffers and the test peptides were injected by a nonpulsatile piston pump into the 30-μl flow cell that was mounted on the coupling prim. Each measurement cycle contained four steps: washing with running buffer containing 10 mM HEPES, pH 7.4, 150 mM NaCl, 3 mM EDTA, and 0.05% Tween 20 at a constant rate of 2 μl/s to obtain a stable baseline, sample injection at 5 μl/s for binding, surface washing with running buffer at 2 μl/s for 300 s, and regeneration with 0.5% (vol/vol) H_3PO_4 at 2 μl/s for 300 s. All the measurements were performed at 25°C. The signal changes after binding and washing (in AU) are recorded as the assay value.

Kinetics fitting and analysis. Selected protein-grafted regions in the SPR images were analyzed, and the average reflectivity variations of the chosen areas were plotted as a function of time. Real-time binding signals were recorded and analyzed by the Data Analysis Module (DAM; Plexera Bioscience, Seattle, WA, USA). Kinetic analysis was performed using BIAevaluation 4.1 software (Biacore, Inc.). The resulting data were fit to a 1:1 binding model using Biacore evaluation software (GE Healthcare).

Plasma stability study. The plasma stability study was performed by Creative Biolabs (New York, NY, USA). In brief, the pooled frozen human plasma (BioIVT, United Kingdom) was thawed in a water bath at 37°C prior to the experiment. Plasma was centrifuged at 4,000 rpm for 5 min, and the clots, if any, were removed. The pH was adjusted to 7.4 ± 0.1 if required. A 1 mM stock solution of the peptides was prepared with water with 5% $NH_3 \cdot H_2O$. A 1 mM intermediate of positive-control propantheline was prepared by diluting 10 μl of the stock solution with 90 μl ultrapure water. For control, a 100 μM dosing solution was prepared by diluting 10 μl of the intermediate solution (1 mM) with 90 μl 45% MeOH/H_2O. For test peptide, 100 μM dosing solution was prepared by diluting 10 μl of the intermediate solution (1 mM) with 90 μl dimethyl sulfoxide (DMSO). Ninety-eight microliters of blank plasma was spiked with 2 μl of dosing solution (100 μM) to achieve 2 μM final concentration in duplicate, and samples were Incubated at 37°C in a water bath. At each time point (0, 10, 30, 60, and 120 min), 100 μl 4% H_3PO_4 was added first, and then 800 μl of stop solution (200 ng/ml tolbutamide and 200 ng/ml labetalol in MeOH) was added to precipitate protein and mixed thoroughly. Sample plates were centrifuged at 4,000 rpm for 10 min. An aliquot of supernatant (100 μl) was transferred from each well to the plate. The samples were shaken at 800 rpm for about 10 min before submission to LC-MS/MS analysis. The percent remaining of the test peptides after incubation in plasma was calculated using the following equation: % remaining = 100 × (PAR at appointed incubation time/PAR at time zero), where PAR is the peak area ratio of analyte versus internal standard (IS).

Cells and plasmids. The human lung carcinoma cells (A549) expressing human angiotensin-converting enzyme 2 (hemagglutinin [HA]-FLAG) (catalog no. NR-53522) were obtained from BEI Resources, NIAID, NIH. HeLa, A549, HT1080, and HEK293T/17 cells were purchased from ATCC (Manassas, VA). The HT1080/ACE2 (human fibrosarcoma) cells and the two plasmids pNL4-3ΔEnv-NanoLuc and pSARS-CoV-2-S$_{\Delta 19}$ were kindly provided by Paul Bieniasz of Rockefeller University (30). The pHEF-VSV-G envelope expression vector (34) and the Env-deleted proviral backbone plasmid pNL4-3.Luc.R-E- DNA (35, 36) was obtained through the NIH AIDS Reagent Program (ARP).

Pseudovirus preparation. To prepare pseudoviruses capable of single-cycle infection, 10×10^6 HEK293T/17 cells were transfected with a proviral backbone plasmid and an envelope expression vector by using FuGENE6 (Promega, Madison, WI) and following the manufacturer's instructions. To obtain the SARS-CoV-2 pseudovirus, the cells were transfected with the HIV-1 Env-deleted proviral backbone plasmid pNL4-3ΔEnv-NanoLuc DNA and the pSARS-CoV-2-S$_{\Delta 19}$ plasmid (30). For the VSV-G pseudovirus, the cells were transfected with the Env-deleted proviral backbone plasmid pNL4-3.Luc.R-E- DNA and the pHEF-VSV-G envelope expression vector. Pseudovirus-containing supernatants were collected 2 days after transfection and filtered, their titers were determined, and they were stored in aliquots at −80°C. Pseudovirus titers were determined to identify the 50% tissue culture infectious dose (TCID$_{50}$) by

infecting different cell types. For the titers in HT1080/ACE2 cells, 2×10^4 cells were added to 100-μl aliquots of serial 2-fold dilutions of pseudoviruses in a 96-well plate and incubated for 24 h. For the titers in A549/ACE2 cells, 1×10^4 cells were added to 100-μl aliquots of serial 2-fold dilutions of pseudoviruses in a 96-well plate and incubated for 48 h. Following the incubation time, the cells were washed with PBS and lysed with 50 μl of the cell culture lysis reagent (Promega, Madison, WI). For the SARS-CoV-2 titers, 25 μl of the lysates was transferred to a white plate and mixed with the same volume of Nano-Glo luciferase reagent (Promega). For the VSV-G titers, 25 μl of the lysates was transferred to a white plate and mixed with 50 μl of luciferase assay reagent (luciferase assay system, Promega). We immediately measured the luciferase activity with a Tecan Spark multifunctional microplate reader (Tecan, Research Triangle Park, NC). The wells producing relative luminescence unit (RLU) levels 10 times the cell background were scored as positive. We calculated the TCID$_{50}$ according to the Spearman-Karber method (37).

Analysis of the incorporation of spike proteins into SARS-CoV-2 pseudovirus. To confirm the incorporation of the spike protein into the SARS-CoV-2 pseudovirus, 2 ml of the pseudovirus-containing supernatant was ultracentrifuged for 2 h at 38,000 rpm on a 20% sucrose cushion to concentrate the viral particles. Viral pellets were lysed and processed for protein analysis. The viral proteins were resolved on a NuPAGE Novex 4 to 12% Bis-Tris gel (Invitrogen, Carlsbad, CA) and immunodetected with a SARS spike protein antibody (NB-100-56578; Novus Biological, Littleton, CO). An anti-rabbit-IgG horseradish peroxidase (HRP)-linked whole antibody (GE Healthcare, Chicago, IL) was used as a secondary antibody. Proteins were visualized using chemiluminescence. Additionally, the correlation of the pseudovirus SARS-CoV-2 with the expression of the ACE2 receptor was analyzed by infecting five different cell types expressing different amounts of the ACE2 receptor with the same volume of the pseudovirus-containing supernatant. Briefly, 50 μl of SARS-CoV-2 diluted with 50 μl serum-free medium was added to wells of a 96-well cell culture plate. Next, the cells were added as follows: HT1080\ACE2 and HT1080 cells were added to the respective wells at the concentration of 2×10^4 cells/well and incubated for 24 h at 37°C; A549\ACE2, A549, and HeLa cells were added to the respective wells at a concentration of 1×10^4 cells/well and incubated for 48 h at 37°C. Uninfected cells for all cell lines were used as a negative control. Following the incubation time, the cells were washed with PBS and lysed with 50 μl of the cell culture lysis reagent. Twenty-five microliters of the lysates was transferred to a white plate and mixed with the same volume of Nano-Glo luciferase reagent. The luciferase activity was immediately measured with a Tecan Spark.

Evaluation of the ACE2 expression in different cell lines. The expression levels of the ACE2 receptor was evaluated by Western blotting to find a correlation with the infection levels detected in the five cell lines HT1080\ACE2, HT1080, A549\ACE2, A549, and HeLa. Cell pellets were lysed and processed for protein analysis. For Blot-1, we loaded 50 μg of proteins (medium, HeLa, HT1080, HT1080/ACE2), and for Blot-2, we loaded 75 μg of proteins (medium, HeLa, A549, and A549/ACE2). The proteins were resolved on a NuPAGE Novex 4 to 12% Bis-Tris gel and immunodetected with a human anti-ACE2 MAb (AC384) (AdipoGen Life Sciences, San Diego, CA). The enhanced chemiluminescence (ECL) mouse IgG, HRP-linked whole Ab (from sheep) (Amersham, Little Chalfont, United Kingdom) was used as a secondary antibody. Proteins were also immunodetected with the housekeeping gene β-actin as a loading control. Proteins were visualized using chemiluminescence.

Measurement of antiviral activity. (i) HT1080/ACE2 cells. The antiviral activity of the peptides was evaluated in single-cycle infection assay by infecting HT1080/ACE2 cells with the SARS-CoV-2 pseudovirus, as previously described with minor modifications (31). Briefly, in 96-well culture plates, aliquots of SARS-CoV-2 at about 3,000 TCID$_{50}$/well at a multiplicity of infection (MOI) of 0.1 were preincubated with escalating concentrations of the peptides for 30 min. Next, 2×10^4 cells were added to each well and incubated at 37°C. HT1080/ACE2 cells cultured with medium with or without the SARS-CoV-2 pseudovirus were included as positive and negative controls, respectively. The linear peptide NYBSP-C, StRIP16 (29) (Tocris, Bristol, United Kingdom), which is a SARS-CoV-2-unrelated Rab8a GTPase-binding double-stapled peptide, and an anti-ACE2 MAb (AC384; catalog no. AG-20A-0037PF; AdipoGen Life Sciences, San Diego, CA) were used as controls. In the case of the anti-ACE2 MAb, the cells were preincubated with escalating concentrations of the MAb for 30 min and then infected with the pseudovirus SARS-CoV-2. Following 24 h of incubation, the cells were washed with 100 μl of PBS and lysed with 50 μl of lysis buffer (Promega). Twenty-five microliters of the lysates was transferred to a white plate and mixed with the same volume of Nano-Glo luciferase reagent (Promega). The luciferase activity was measured immediately with the Tecan Spark. The percent inhibition by the peptides and the IC$_{50}$ (the half-maximal inhibitory concentration) values were calculated using GraphPad Prism 7.0 software (San Diego, CA). Additionally, to test the specificity of the double-stapled peptides, we evaluated their activity against pseudovirus VSV-G by following the infection protocol described above. Following 24 h of incubation, 25 μl of the lysates was transferred to a white plate and mixed with 50 μl of a luciferase assay reagent. The luciferase activity was immediately measured.

(ii) A549/ACE2 cells. For the evaluation of the antiviral activity in A549/ACE2 cells, aliquots of the pseudovirus SARS-CoV-2 at about 1,500 TCID$_{50}$/well at an MOI of 0.1 were preincubated with escalating concentrations of the double-stapled peptides for 30 min. Next, 1×10^4 cells were added to each well and incubated. A549/ACE2 cells cultured with medium with or without the SARS-CoV-2 pseudovirus were included as positive and negative controls, respectively. The linear peptide NYBSP-C, the double-stapled peptide StRIP16, and the anti-ACE2 MAb were used as controls. In the case of the anti-ACE2 MAb, the cells were preincubated with escalating concentrations of the Ab for 30 min and then infected with the pseudovirus SARS-CoV-2. Following 48 h of incubation, the cells were washed with PBS and lysed with 50 μl of lysis buffer. Twenty-five microliters of the cell lysates was processed as reported above to measure the luciferase activity and calculate the percent inhibition by the peptides and the

IC_{50}. Moreover, the double-stapled peptides were evaluated against pseudovirus VSV-G by following the infection protocol described above. Following 48 h of incubation, 25 μl of the lysates was transferred to a white plate and mixed with 50 μl of a luciferase assay reagent. The luciferase activity was immediately measured.

SARS-CoV-2 MN assay. The standard live virus-based microneutralization (MN) assay was used (38–40). Briefly, serially 2-fold-diluted and duplicate dilutions of individual peptides were incubated with 120 PFU of SARS-CoV-2 (US_WA-1/2020) at room temperature for 1 h before transferring into designated wells of confluent Vero E6 cells (ATCC, CRL-1586) grown in 96-well cell culture plates. Vero E6 cells cultured with medium with or without the same amount of virus were included as positive and negative controls, respectively. After incubation at 37°C for 3 to 4 days, individual wells were observed under the microscope to determine the virus-induced formation of cytopathic effect (CPE). The efficacy of individual drugs was expressed as the lowest concentration capable of completely preventing virus-induced CPE in 100% of the wells.

Evaluation of cytotoxicity. (i) HT1080/ACE2 cells. The evaluation of the cytotoxicity of the peptides in HT1080/ACE2 cells was performed in parallel with the antiviral activity assay and measured by using the colorimetric CellTiter 96 Aqueous One Solution cell proliferation assay {MTS [3-(4,5-dimethylthiazol-2-yl)-5-(3-carboxymethoxyphenyl)-2-(4-sulfophenyl)-2H-tetrazolium]} (Promega, Madison, WI) following the manufacturer's instructions. Briefly, aliquots of 100 μl of the peptides at graded concentrations were incubated with 2×10^4/well HT1080/ACE2 cells and cultured at 37°C. Following 24 h of incubation, the MTS reagent was added to the cells and incubated for 4 h at 37°C. The absorbance was recorded at 490 nm. The percentage of cytotoxicity and the CC_{50} (the concentration for 50% cytotoxicity) values were calculated as described above.

(ii) A549/ACE2 cells. For the cytotoxicity assay in A549/ACE2 cells, aliquots of escalating concentrations of the peptides were incubated with 1×10^4/well A549/ACE2 cells and cultured at 37°C. Following 48 h of incubation, the MTS reagent was added to the cells and incubated for 4 h at 37°C. The absorbance was recorded at 490 nm. The percentage of cytotoxicity and the CC_{50} values were calculated as described above.

Conclusions. The current pandemic made it urgent to develop therapeutics against COVID-19. We took advantage of the structural knowledge of the binding site of SARS-CoV-2 RBD and the ACE2 receptor. We envisioned that a stapled peptide based on the helix region of ACE2 that binds with the SARS-CoV-2 RBD might work as a decoy receptor, bind SARS-CoV-2 preferentially, and prevent its entry into the host cells and thereby the subsequent infection by the virus. We reported the successful design of double-stapled peptides with potent antiviral activity in HT1080/ACE2 and human lung carcinoma cells, A549/ACE2. Most significantly, all three active stapled peptides with potent antiviral activity against SARS-CoV-2 pseudovirus showed high helical content (60 to 94%). We also evaluated the antiviral activity of the peptides by infecting Vero E6 cells with the replication-competent authentic SARS-CoV-2 (US_WA-1/2020). NYBSP-1, NYBSP-2, and NYBSP-4 completely (IC_{100}) inhibited virus-induced CPE at low-micromolar doses. One of the most active stapled peptides, NYBSP-4, demonstrated a binding affinity (K_D) of 2.2 μM with SARS-CoV-2 RBD, which was in line with the antiviral activity of the stapled peptide against SARS-CoV-2 pseudovirus. NYBSP-4 also showed substantial resistance to degradation by proteolytic enzymes in human plasma. The lead stapled peptides are expected to pave the way for further optimization of a clinical candidate.

REFERENCES

1. Batlle D, Wysocki J, Satchell K. 2020. Soluble angiotensin-converting enzyme 2: a potential approach for coronavirus infection therapy? Clin Sci (Lond) 134:543–545. https://doi.org/10.1042/CS20200163.
2. EU Clinical Trials Register. 2020. Recombinant human angiotensin-converting enzyme 2 (rhACE2) as a treatment for patients with COVID-19. https://www.clinicaltrialsregister.eu/ctr-search/search?query=eudract_number2020-001172-15.
3. Wysocki J, Ye M, Rodriguez E, Gonzalez-Pacheco FR, Barrios C, Evora K, Schuster M, Loibner H, Brosnihan KB, Ferrario CM, Penninger JM, Batlle D. 2010. Targeting the degradation of angiotensin II with recombinant angiotensin-converting enzyme 2: prevention of angiotensin II-dependent hypertension. Hypertension 55:90–98. https://doi.org/10.1161/HYPERTENSIONAHA.109.138420.
4. Haschke M, Schuster M, Poglitsch M, Loibner H, Salzberg M, Bruggisser M, Penninger J, Krahenbuhl S. 2013. Pharmacokinetics and pharmacodynamics of recombinant human angiotensin-converting enzyme 2 in healthy human subjects. Clin Pharmacokinet 52:783–792. https://doi.org/10.1007/s40262-013-0072-7.
5. Lei C, Qian K, Li T, Zhang S, Fu W, Ding M, Hu S. 2020. Neutralization of SARS-CoV-2 spike pseudotyped virus by recombinant ACE2-Ig. Nat Commun 11:2070. https://doi.org/10.1038/s41467-020-16048-4.
6. Zhang G, Pomplun S, Loftis AR, Tan X, Loas A, Pentelute BL. 2020. The first-in-class peptide binder to the SARS-CoV-2 spike protein. bioRxiv https://doi.org/10.1101/2020.03.19.999318. Accessed 20 March 2020.
7. Walls AC, Park YJ, Tortorici MA, Wall A, McGuire AT, Veesler D. 2020. Structure, function, and antigenicity of the SARS-CoV-2 spike glycoprotein. Cell 181:281–292.e6. https://doi.org/10.1016/j.cell.2020.02.058.
8. Wrapp D, Wang N, Corbett KS, Goldsmith JA, Hsieh CL, Abiona O, Graham BS, McLellan JS. 2020. Cryo-EM structure of the 2019-nCoV spike in the prefusion conformation. Science 367:1260–1263. https://doi.org/10.1126/science.abb2507.
9. Lan J, Ge J, Yu J, Shan S, Zhou H, Fan S, Zhang Q, Shi X, Wang Q, Zhang L, Wang X. 2020. Structure of the SARS-CoV-2 spike receptor-binding domain bound to the ACE2 receptor. Nature 581:215–220. https://doi.org/10.1038/s41586-020-2180-5.
10. Shang J, Ye G, Shi K, Wan Y, Luo C, Aihara H, Geng Q, Auerbach A, Li F.

2020. Structural basis of receptor recognition by SARS-CoV-2. Nature 581:221–224. https://doi.org/10.1038/s41586-020-2179-y.

11. Ali AM, Atmaj J, Van Oosterwijk N, Groves MR, Domling A. 2019. Stapled peptides inhibitors: a new window for target drug discovery. Comput Struct Biotechnol J 17:263–281. https://doi.org/10.1016/j.csbj.2019.01.012.

12. Iegre J, Ahmed NS, Gaynord JS, Wu Y, Herlihy KM, Tan YS, Lopes-Pires ME, Jha R, Lau YH, Sore HF, Verma C, Donovan DHO, Pugh N, Spring DR. 2018. Stapled peptides as a new technology to investigate protein-protein interactions in human platelets. Chem Sci 9:4638–4643. https://doi.org/10.1039/c8sc00284c.

13. Moiola M, Memeo MG, Quadrelli P. 2019. Stapled peptides—a useful improvement for peptide-based drugs. Molecules 24:3654. https://doi.org/10.3390/molecules24203654.

14. Muppidi A, Zhang H, Curreli F, Li N, Debnath AK, Lin Q. 2014. Design of antiviral stapled peptides containing a biphenyl cross-linker. Bioorg Med Chem Lett 24:1748–1751. https://doi.org/10.1016/j.bmcl.2014.02.038.

15. Charoenpattarapreeda J, Tan YS, Iegre J, Walsh SJ, Fowler E, Eapen RS, Wu Y, Sore HF, Verma CS, Itzhaki L, Spring DR. 2019. Targeted covalent inhibitors of MDM2 using electrophile-bearing stapled peptides. Chem Commun (Camb) 55:7914–7917. https://doi.org/10.1039/c9cc04022f.

16. Cowell JK, Teng Y, Bendzunas NG, Ara R, Arbab AS, Kennedy EJ. 2017. Suppression of breast cancer metastasis using stapled peptides targeting the WASF regulatory complex. Cancer Growth Metastasis 10:1179064417713197. https://doi.org/10.1177/1179064417713197.

17. Cromm PM, Spiegel J, Grossmann TN. 2015. Hydrocarbon stapled peptides as modulators of biological function. ACS Chem Biol 10:1362–1375. https://doi.org/10.1021/cb501020r.

18. Dietrich L, Rathmer B, Ewan K, Bange T, Heinrichs S, Dale TC, Schade D, Grossmann TN. 2017. Cell permeable stapled peptide inhibitor of Wnt signaling that targets beta-catenin protein-protein interactions. Cell Chem Biol 24:958–968.e5. https://doi.org/10.1016/j.chembiol.2017.06.013.

19. Dougherty PG, Wen J, Pan X, Koley A, Ren JG, Sahni A, Basu R, Salim H, Appiah Kubi G, Qian Z, Pei D. 2019. Enhancing the cell permeability of stapled peptides with a cyclic cell-penetrating peptide. J Med Chem 62:10098–10107. https://doi.org/10.1021/acs.jmedchem.9b00456.

20. Gaillard V, Galloux M, Garcin D, Eleouet JF, Le Goffic R, Larcher T, Rameix-Welti MA, Boukadiri A, Heritier J, Segura JM, Baechler E, Arrell M, Mottet-Osman G, Nyanguile O. 2017. A short double-stapled peptide inhibits respiratory syncytial virus entry and spreading. Antimicrob Agents Chemother 61:e02241-16. https://doi.org/10.1128/AAC.02241-16.

21. Verdine GL, Hilinski GJ. 2012. Stapled peptides for intracellular drug targets. Methods Enzymol 503:3–33. https://doi.org/10.1016/B978-0-12-396962-0.00001-X.

22. Aileron Therapeutics, Inc. 2020. Clinical programs: ALRN-6924. Aileron Therapeutics, Inc, Watertown, MA. https://www.aileronrx.com/clinical-development/.

23. Mourtada R, Herce HD, Yin DJ, Moroco JA, Wales TE, Engen JR, Walensky LD. 2019. Design of stapled antimicrobial peptides that are stable, nontoxic and kill antibiotic-resistant bacteria in mice. Nat Biotechnol 37:1186–1197. https://doi.org/10.1038/s41587-019-0222-z.

24. Ran X, Liu L, Yang CY, Lu J, Chen Y, Lei M, Wang S. 2016. Design of high-affinity stapled peptides to target the repressor activator protein 1 (RAP1)/telomeric repeat-binding factor 2 (TRF2) protein-protein interaction in the shelterin complex. J Med Chem 59:328–334. https://doi.org/10.1021/acs.jmedchem.5b01465.

25. Bird GH, Crannell WC, Walensky LD. 2011. Chemical synthesis of hydrocarbon-stapled peptides for protein interaction research and therapeutic targeting. Curr Protoc Chem Biol 3:99–117. https://doi.org/10.1002/9780470559277.ch110042.

26. Walensky LD, Kung AL, Escher I, Malia TJ, Barbuto S, Wright RD, Wagner G, Verdine GL, Korsmeyer SJ. 2004. Activation of apoptosis in vivo by a hydrocarbon-stapled BH3 helix. Science 305:1466–1470. https://doi.org/10.1126/science.1099191.

27. Walensky LD, Bird GH. 2014. Hydrocarbon-stapled peptides: principles, practice, and progress. J Med Chem 57:6275–6288. https://doi.org/10.1021/jm4011675.

28. Bird GH, Madani N, Perry AF, Princiotto AM, Supko JG, He X, Gavathiotis E, Sodroski JG, Walensky LD. 2010. Hydrocarbon double-stapling remedies the proteolytic instability of a lengthy peptide therapeutic. Proc Natl Acad Sci U S A 107:14093–14098. https://doi.org/10.1073/pnas.1002713107.

29. Cromm PM, Spiegel J, Kuchler P, Dietrich L, Kriegesmann J, Wendt M, Goody RS, Waldmann H, Grossmann TN. 2016. Protease-resistant and cell-permeable double-stapled peptides targeting the Rab8a GTPase. ACS Chem Biol 11:2375–2382. https://doi.org/10.1021/acschembio.6b00386.

30. Schmidt F, Weisblum Y, Muecksch F, Hoffmann HH, Michailidis E, Lorenzi JCC, Mendoza P, Rutkowska M, Bednarski E, Gaebler C, Agudelo M, Cho A, Wang Z, Gazumyan A, Cipolla M, Caskey M, Robbiani DF, Nussenzweig MC, Rice CM, Hatziioannou T, Bieniasz PD. 2020. Measuring SARS-CoV-2 neutralizing antibody activity using pseudotyped and chimeric viruses. J Exp Med 217:e20201181. https://doi.org/10.1084/jem.20201181.

31. Nie J, Li Q, Wu J, Zhao C, Hao H, Liu H, Zhang L, Nie L, Qin H, Wang M, Lu Q, Li X, Sun Q, Liu J, Fan C, Huang W, Xu M, Wang Y. 2020. Establishment and validation of a pseudovirus neutralization assay for SARS-CoV-2. Emerg Microbes Infect 9:680–686. https://doi.org/10.1080/22221751.2020.1743767.

32. Smith TRF, Patel A, Ramos S, Elwood D, Zhu X, Yan J, Gary EN, Walker SN, Schultheis K, Purwar M, Xu Z, Walters J, Bhojnagarwala P, Yang M, Chokkalingam N, Pezzoli P, Parzych E, Reuschel EL, Doan A, Tursi N, Vasquez M, Choi J, Tello-Ruiz E, Maricic I, Bah MA, Wu Y, Amante D, Park DH, Dia Y, Ali AR, Zaidi FI, Generotti A, Kim KY, Herring TA, Reeder S, Andrade VM, Buttigieg K, Zhao G, Wu JM, Li D, Bao L, Liu J, Deng W, Qin C, Brown AS, Khoshnejad M, Wang N, Chu J, Wrapp D, McLellan JS, Muthumani K, Wang B, Carroll MW, Kim JJ, Boyer J, Kulp DW, Humeau LMPF, Weiner DB, Broderick KE. 2020. Immunogenicity of a DNA vaccine candidate for COVID-19. Nat Commun 11:2601. https://doi.org/10.1038/s41467-020-16505-0.

33. Bohm G, Muhr R, Jaenicke R. 1992. Quantitative analysis of protein far UV circular dichroism spectra by neural networks. Protein Eng 5:191–195. https://doi.org/10.1093/protein/5.3.191.

34. Chang LJ, Urlacher V, Iwakuma T, Cui Y, Zucali J. 1999. Efficacy and safety analyses of a recombinant human immunodeficiency virus type 1 derived vector system. Gene Ther 6:715–728. https://doi.org/10.1038/sj.gt.3300895.

35. Connor RI, Chen BK, Choe S, Landau NR. 1995. Vpr is required for efficient replication of human immunodeficiency virus type-1 in mononuclear phagocytes. Virology 206:935–944. https://doi.org/10.1006/viro.1995.1016.

36. He J, Choe S, Walker R, Di Marzio P, Morgan DO, Landau NR. 1995. Human immunodeficiency virus type 1 viral protein R (Vpr) arrests cells in the G2 phase of the cell cycle by inhibiting p34cdc2 activity. J Virol 69:6705–6711. https://doi.org/10.1128/JVI.69.11.6705-6711.1995.

37. HIV/AIDS Network Coordination. 2004. TCID50 (50% tissue culture infectious dose) determination. Quantitation of viable HIV-1 virions in culture supernatants. HIV/AIDS Network Coordination, Seattle, WA. https://www.hanc.info/labs/labresources/procedures/ACTGIMPAACT%20Lab%20Manual%20Archive/TCID50%20Determination%20-%20ARCHIVED_WM.pdf.

38. Li W, Schafer A, Kulkarni SS, Liu X, Martinez DR, Chen C, Sun Z, Leist SR, Drelich A, Zhang L, Ura ML, Berezuk A, Chittori S, Leopold K, Mannar D, Srivastava SS, Zhu X, Peterson EC, Tseng CT, Mellors JW, Falzarano D, Subramaniam S, Baric RS, Dimitrov DS. 2020. High potency of a bivalent human VH domain in SARS-CoV-2 animal models. Cell 183:429–441.e16. https://doi.org/10.1016/j.cell.2020.09.007.

39. Du L, Zhao G, Yang Y, Qiu H, Wang L, Kou Z, Tao X, Yu H, Sun S, Tseng CT, Jiang S, Li F, Zhou Y. 2014. A conformation-dependent neutralizing monoclonal antibody specifically targeting receptor-binding domain in Middle East respiratory syndrome coronavirus spike protein. J Virol 88:7045–7053. https://doi.org/10.1128/JVI.00433-14.

40. Agrawal AS, Ying T, Tao X, Garron T, Algaissi A, Wang Y, Wang L, Peng BH, Jiang S, Dimitrov DS, Tseng CT. 2016. Passive Transfer of a germline-like neutralizing human monoclonal antibody protects transgenic mice against lethal Middle East respiratory syndrome coronavirus infection. Sci Rep 6:31629. https://doi.org/10.1038/srep31629.